Title	Characterization of microstructural defects in melt grown ZnO single crystals
Author(s)	Anwand, W; Brauer, G; Grynszpan, RI; Cowan, TE; Schulz, D; Klimm, D; Iek, J; Kuriplach, J; Prochzka, I; Ling, CC; Djurii, AB; Klemm, V; Schreiber, G; Rafaja, D
Citation	Journal Of Applied Physics, 2011, v. 109 n. 6
Issued Date	2011
URL	http://hdl.handle.net/10722/134642
Rights	Journal of Applied Physics. Copyright © American Institute of Physics.

Characterization of microstructural defects in melt grown ZnO single crystals

W. Anwand,[1,a)] G. Brauer,[1] R. I. Grynszpan,[1] T. E. Cowan,[1] D. Schulz,[2] D. Klimm,[2] J. Čížek, [3] J. Kuriplach,[3] I. Procházka,[3] C. C. Ling,[4] A. B. Djurišić,[4] V. Klemm,[5] G. Schreiber,[5] and D. Rafaja[5]

[1]*Institut für Strahlenphysik, Helmholtz-Zentrum Dresden-Rossendorf, Postfach 510119, D-01314 Dresden, Germany*

[2]*Institut für Kristallzüchtung, Max-Born-Str. 2, D-12489 Berlin, Germany*

[3]*Department of Low Temperature Physics, Faculty of Mathematics and Physics, Charles University, V Holešovičkách 2, CZ- 180 00 Prague, Czech Republic*

[4]*Department of Physics, University of Hong Kong, Pokfulam Road, Hong Kong, People's Republic of China*

[5]*Institute of Materials Science, TU Bergakademie Freiberg, Gustav-Zeuner-Str. 5, D-09599 Freiberg, Germany*

(Received 5 November 2010; accepted 21 January 2011; published online 22 March 2011)

Various nominally undoped, hydrothermally or melt grown (MG) ZnO single crystals have been investigated by standard positron lifetime measurements. Furthermore, optical transmission measurements and structural characterizations have been performed; the content of hydrogen in the bound state was determined by nuclear reaction analysis. A positron lifetime of 165-167 ps, measured for a brownish MG ZnO sample containing (0.30 ± 0.03) at.-% of bound hydrogen, matches perfectly the value found for colorless MG ZnO crystals. The edge shift, observed in the "blue light domain" of the optical absorption for the former sample with respect to the latter samples, is estimated to be 0.70 eV, and found equal to a value reported previously. The possible role of zinc interstitials is considered and discussed. Microstructure analysis by X-ray diffraction and transmission electron microscopy revealed the presence of stacking faults in MG crystals in a high concentration, which suggests these defects to be responsible for the observed positron lifetime. © *2011 American Institute of Physics*. [doi:10.1063/1.3559264]

I. INTRODUCTION

Differences in the physical properties of ZnO crystals reported in the scientific literature are mainly related to the native defects formed during crystal growth.[1–4] Recently, the effect of the microstructure defects on the electronic properties was investigated by means of positron annihilation spectroscopy (PAS) that employed either the standard ^{22}Na source technique[5,6] or a variable positron energy beam.[7,8]

A systematic PAS study[9] of various, nominally undoped, ZnO single crystals revealed the single positron lifetimes of 180-182 ps in crystals that were hydrothermally grown (HTG) and 165-167 ps in crystals that were grown from the melt (MG). In all crystals, a high concentration of hydrogen in a bound state (at least 0.3 at.-%) has been detected by nuclear reaction analysis (NRA). The concentration of other impurities was low, as detected by inductively coupled plasma mass spectrometry (ICP-MS).

From *ab initio* calculations[9] it has been inferred that the saturation trapping at $V_{Zn} + 1H$ defects is the most natural explanation for the 180-182 ps positron lifetime observed in HTG crystals. Conversely, it has been concluded that the $V_{Zn} + 2H$ and $V_{Zn} + 3H$ defects do not trap positrons, and thus they cannot explain the 165–167 ps positron lifetime found in all MG crystals investigated so far. It is possible that structurally more complicated H-vacancy complexes might explain the measured lifetime. However, relevant *ab initio* calculations are not straightforwardly achievable.

All our HTG and MG crystals investigated previously by PAS[9] were colorless and transparent in their as-received state. However, the researchers from the IKZ Berlin[10] reported that their MG crystals had a color ranging from orange to brownish, and exhibited a large number of micrometer-sized precipitates visible even by optical microscopy. While the chemical nature of these precipitates could not be revealed, they tended to vanish after annealing at 900 °C in ambient air for 18 h and the crystals became almost colorless. Thus, a next consequential task was to investigate if precipitates or other possible microstructure defects, like stacking faults, exist in a sufficiently large concentration to be able to cause saturation trapping of positrons in MG crystals and hence to provide a more solid alternative explanation for the occurrence of the 165-167 ps lifetime.

To verify this hypothesis positron lifetime measurements were performed on such a pair of MG crystals of brownish color.[10] These measurements were complemented by ICP-MS analysis to determine the content of impurities. In addition, to account for the possible influence of hydrogen on the ZnO properties - currently debated in the literature[11–17] - the actual H content in this crystal was estimated by NRA.

These results, and those of additional optical transmission measurements, were then used for comparison with those obtained for colorless and transparent HTG and MG crystals studied previously.[9]

Furthermore, the possible role of zinc interstitials is considered and discussed. Finally, X-ray diffraction (XRD) and transmission electron microscopy (TEM) were performed to

a)Electronic mail: w.anwand@hzdr.de.

assess the microstructure of the samples and to clarify the presence of stacking faults in MG crystals in particular.

II. EXPERIMENTAL

Single crystals of typical dimensions of $10 \times 10 \times 0.5$ mm^3 used here have been investigated previously.[9,17] HTG samples were supplied by MaTecK GmbH (Jülich) (MT-06, MT-08), with their O-face polished. MG crystals originated from Cermet Inc. (Atlanta-GA) (CM-06) and IKZ (Berlin) (B12, B13). The crystals from Cermet Inc., were grown without using a crucible[18,19] and the IKZ crystals by using the Bridgman method.[10] A pair of MG crystals from the same boule (B5) having brownish color[10] has been supplied by IKZ (Berlin).

ICP-MS was performed using a Perkin-Elmer ELAN-9000 spectrometer. The possibility to determine the H content by standard NRA[20] using 6.64 MeV ^{15}N ions has already been successfully demonstrated for HTG ZnO nanorods[21] and for HTG and MG ZnO crystals[9,17] in connection with SRIM calculations ("The Stopping and Range of Ions in Matter" - software [22]). A straggling (depth resolution) of ~5 nm at a depth of ~100 nm guarantees a negligible influence of surface contaminations. The amount of H measured with a detection limit of ~200 ppm is then assumed to represent volume properties.

The microstructure of the crystals B5, B13 and MT-08 has been investigated by using XRD and TEM. Overview XRD measurements were carried out on a conventional Bragg-Brentano diffractometer that was equipped with a sealed X-ray tube with a Cu anode and with a secondary curved graphite monochromator.

High-resolution XRD comprising reciprocal space mapping and sample scans (Ω scans) was performed using a triple-crystal diffractometer equipped with a sealed X-ray tube with a Cu anode and with a (111) oriented Si monochromator located in the primary beam. The monochromator lets pass only the spectral line $CuK\alpha_1$ to the sample. The third crystal was a (111) oriented Si analyzer located in front of a scintillation detector. In the high-resolution mode, the size of the primary beam was reduced to 1×0.09 mm^2. Consequently, the irradiated area on the sample surface was approximately 1×0.30 mm^2 for the 002 and 104 reflections and 1×0.15 mm^2 for the 004 reflection.

TEM was performed on a transmission electron microscope JEM 2010 FEF from JEOL that was operated at 200 kV, with FEF meaning field emission gun (F) and omega energy filter (EF). The samples for TEM were prepared in the plan-view orientation. This means that the primary electron beam was parallel to the $\langle 001 \rangle$ direction of the crystal. The first step in the TEM sample preparation was mechanical prethinning that was followed by etching in an Ar ion beam.

The state-of-the-art positron lifetime (LT) measurements were performed at room temperature by a fast- fast spectrometer having a timing resolution of 160 ps (Ref. 23) and collecting $\sim 10^7$ events per spectrum. A ^{22}Na positron source (~1.5 MBq) deposited on a 2 μm thick Mylar foil has been used. This source was covered with two identically treated ZnO crystals that formed a sandwich. The positron source contribution in the LT spectra consisted of two weak components with lifetimes of ~368 ps and ~1.5 ns, and corresponding intensities of ~8% and ~1%, respectively. Each LT spectrum has been decomposed using a maximum likelihood procedure described in detail elsewhere.[24]

The optical transmission of all crystals was investigated at IKZ Berlin using a PerkinElmer Lambda 19 spectrometer equipped with a white light source (tungsten halogen lamp) and a grating monochromator. The optical transmission defined as the intensity ratio I/I_0 was generally measured within the wavelength range 200- 2500 nm. I_0 refers to the primary intensity of the light source; I is the intensity of the light after passing through the crystal. The reflectivity of each crystal has been assumed to be independent of the wavelength in first approximation, i.e., no correction of the transmitted amounts of light has been made.

The optical transmission of one of the as-received B5 crystals was measured independently at Charles University, Prague within the limited wavelength range 340-850 nm using a Spekol spectrometer equipped with a white light source and a mesh monochromator. Again, no correction for the change of reflectivity with the wavelength was performed.

The optical transmission of HTG crystals supplied by MaTecK GmbH (Jülich) (MT-04) was investigated in their as-received state and after irradiation by 10 MeV electrons. The irradiation doses were 1 and 2×10^{18} cm^{-2}, respectively. During irradiation, water cooling ensured that the sample temperature never exceeded 100 °C. More information about the properties of MT-04 samples can be found in Ref. 25.

III. RESULTS AND DISCUSSION

A. ICP-MS, NRA and LT of B5 samples

The chemical composition and H content of all samples investigated is given in Table I. The relation between the atomic concentrations (C_{at}) estimated by ICP-MS and the volume concentrations (C_{vol}) is given by $C_{vol} = C_{at}/\Omega$, where Ω is the average volume per atom in the ZnO lattice. For the ZnO lattice parameters[26] used in previous calculations,[27] a value of $\Omega = 11.91 \times 10^{-24}$ cm^3 is obtained.

From SRIM it was found that the analyzing ^{15}N ions lose their kinetic energy E with increasing penetration depth x mainly by electronic collisions ($[dE/dx]_{electronic} = 2.52$ keV nm^{-1}), whereas the nuclear collision energy loss is about two orders of magnitude smaller ($[dE/dx]_{nuclear} = 0.006$ keV nm^{-1}). The energy transfer to the crystal during the analysis can be sufficient to release a weekly bound hydrogen atom from its bonding site, so that it will be able to start diffusing. It is generally assumed that individual H atoms are too reactive to remain isolated and become bound again immediately, so that this diffusion should most likely take place in the form of H_2 molecules. As this diffusing hydrogen is no longer available at the analysis stage there is a drop in concentration with increasing ^{15}N fluence. Throughout this paper, this will be referred to as "unbound H" (H-u). Conversely, any H atom which is not moving during analysis, because the energy transfer is not sufficient to release it from its bonding site, will be called hereafter "bound H" (H-b). However, it has to be clearly stated that from NRA it

TABLE I. Chemical compositions (volume concentration, in 10^{17} cm^{-3} units) and H content (in at.-%; H-b, H-u stand for H concentrations in 'bound' and 'unbound' states, respectively) of HTG and MG ZnO crystals. '0.00' means that the corresponding element was detected, but rounding gives zero concentration within the given precision; underlined numbers specify upper limits

Sample Element	MT-06	MT-08	CM-06	B12	B13	B5
Li	-	4.06	-	-	0.14	-
Mg	-	1.84	-	-	-	-
Al	80.6	-	-	-	-	2.47
V	-	-	-	-	-	0.00
Cr	-	-	0.01	0.01	0.01	0.00
Mn	0.27	-	-	-	-	-
Co	0.12	-	-	0.03	0.05	-
Ni	1.11	0.65	0.22	0.12	0.13	-
Cu	0.95	1.10	0.34	0.65	0.51	8.49
Ga	-	0.76	0.43	0.60	0.58	1.08
Rb	-	0.02	0.01	0.01	0.01	0.00
Sr	0.09	-	-	-	-	-
Zr	-	-	-	0.09	-	0.00
Mo	-	0.02	0.00	0.00	0.00	-
Ag	-	0.12	0.16	0.17	0.15	-
Cd	0.03	0.33	0.17	-	-	-
In	-	-	1.54	-	-	-
Sn	-	-	0.01	0.46	-	-
Sb	-	-	0.00	0.00	0.00	-
Te	-	0.12	0.04	0.04	0.04	-
Ba	-	0.04	-	-	-	-
Pb	-	0.02	0.09	0.66	0.01	0.03
H-b	0.3	0.2	0.5	0.4	0.5	0.3
H-u	-	-	-	-	0.7	-

is impossible to draw any conclusion on the kind of bonding of H atoms in the crystal.

In the as-received B5 sample, NRA results do not indicate the presence of H in the unbound state (H-u = 0), whereas its content in the bound state amounted to H-b = (0.30 ± 0.03) at.-%. This latter concentration seemed rather stable, since it remains the same after annealing at 500 °C in air for 1 h and after a subsequent storage of the sample at room temperature for a period of 93 days.

Interestingly, the LT measurements of the brownish sample pair B5 revealed an average single positron lifetime of (165.4 ± 0.3) ps, which matches perfectly the 165-167 ps positron lifetime found in all colorless MG crystals investigated previously (see Table II). Owing to the brownish color of B5 samples caused by the presence of precipitates of dimensions visible by optical microscopy, such a match of properties could not be expected at first glance.

B. Optical transmission

In order to obtain an overview of the optical transmission properties of HTG and MG crystals, samples have been investigated within the largest available wavelength range (200–2500 nm). Preliminary data of another B5 sample were taken directly from Ref. 10. Results are presented in Fig. 1.

The transmission of the as-received HTG sample MT-06 has its onset at a wavelength of ~380 nm; then it rises sharply with increasing wavelength to a maximum value of ~80% and continues to increase almost linearly up to ~85% at 2500 nm. At the chosen conditions for the electron irradiation of MT-04 samples, only atomic size defects should be produced, including mono-vacancies, interstitials and perhaps even di-vacancies.

TABLE II. Positron lifetimes for various ZnO samples from this work and the literature (Refs. 9 and 17). Numbers given for MT-06 and MT-08 are averaged from measurements of five different sample pairs

Sample	Growth Method	Positron Lifetime/ps	Reference
MT-06	Hydrothermal Growth	181.7 ± 0.3	9
MT-08	Hydrothermal Growth	180.6 ± 0.5	17
CM-06	Pressurized Melt Growth	166.4 ± 0.4	9
B12	Bridgman Method	165.9 ± 0.2	9
B13	Bridgman Method	166.1 ± 0.3	9
B5	Bridgman Method	165.4 ± 0.3	this work

The transmission is very similar to that of the as-received MT-06 sample, except in the wavelength range 400- 800 nm, where the rise is less steep.

In contrast, the transmission of all as-received MG samples was different in two ways:

(1) After the onset at ~380 nm, the rise is less steep than for sample MT-06; the maximum transmission was in the range 75-80%.

(2) A continuously decreasing transmission was found in the wavelength range 800-2500 nm. This gradual decline in the optical transmission at wavelengths in excess of about 1000 nm is linked to the free carrier concentration, i.e., does not involve the type of point defects produced by electron irradiation.

The drop of transmission in the long wavelength region of the brownish sample B5 has been discussed to be connected with the concentration of free charge carriers too.[10] However, the existence of free charge carriers might also be interpreted in terms of the Zn precipitate formation, which is extremely difficult to be proven directly from experiments. Computer simulations in the framework of the Mie-Lorenz

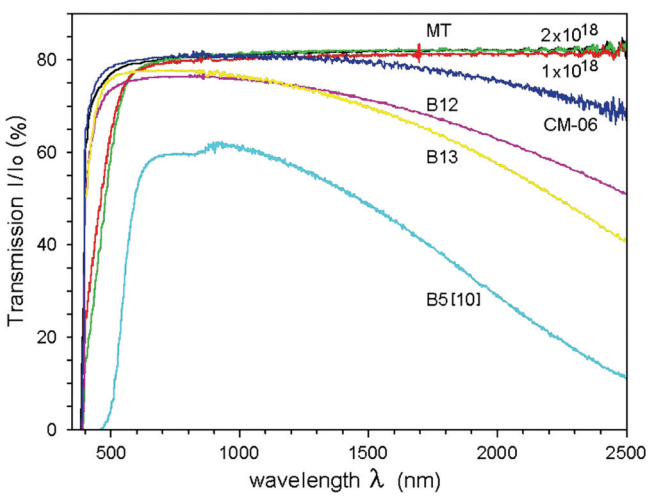

FIG. 1. (Color online) Optical transmission curves in ZnO crystals for various HTG (MT-06 as-received; MT-04 electron-irradiated to 1×10^{18} and 2×10^{18} cm^{-2}) and MG (B12; B13; B5 data are taken from Ref. 10.

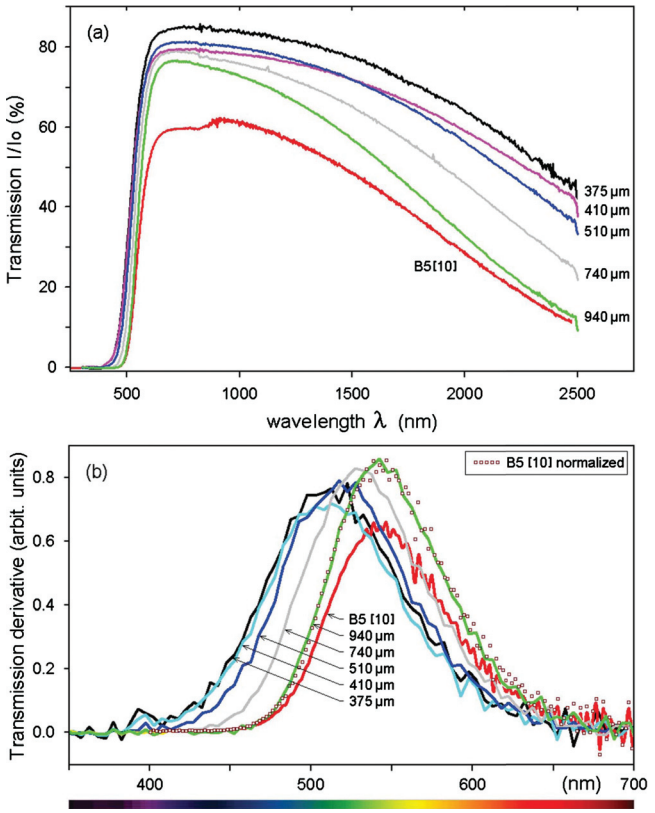

FIG. 2. (Color online) (a) Optical transmission spectra of a new sample B5 measured at various thicknesses, and (b) their derivatives around the "blue" edge with the dotted curve representing the B5 peak (Ref. 10) normalized to the 940 height.

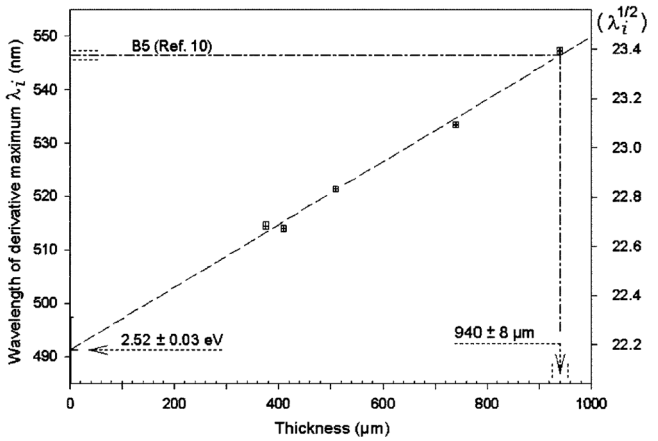

FIG. 3. Linear dependence of the maximum of the optical transmission derivative around the ~500 nm edge on thickness of the position (wavelength λ_i) for a new B5 sample series. The peak positions λ_i displayed on the left hand side axis are estimated from Fig. 2(b) by a Gaussian regression within the 350-700 nm wavelength range. The right hand side axis corresponds to a linear scale of square root values of λ_i. The dash-dotted line indicates the extrapolated thickness for sample B5 from Ref. 10.

theory[28,29] could be helpful but are neither easy nor straightforward to perform.

Although in Ref. 10 it has been mentioned that wafers of a thickness of ~800 µm were prepared, it has not been possible to ascertain afterwards the true thickness of the older B5 sample from which the transmission has been published.

A new B5 sample has been ground from originally 940 µm to various smaller thicknesses (i.e., 740, 510, 410, and 375 µm, respectively, within a ± 5 µm margin error) and polished again prior to the transmission measurements. Hence, five new transmission spectra became available for the B5 series [Fig. 2(a)], labeled hereafter according to their thickness.

The first striking feature is the shift of the ~500 nm edge displayed for the thinned sample series, best evidenced by the thickness dependence of the peak position of the transmission derivative [Fig. 2(b)]. Various procedures were tested to estimate the wavelength associated with each maximum (including fitting to Gaussian, power and lognormal functions); the Gaussian fit proved to be less sensitive to the considered wavelength range. Figure 3 displays the calculated values within the wavelength range 350-700 nm.

This approach revealed the following:

(1) For the five known sample thicknesses (375, 410, 510, 740, and 940 µm), the shift of the transmission edge seems to follow a linear trend (intercept 492 ± 6 nm, goodness of fit parameter 0.993). A similar fit is also found for the linear dependence of the wavelength square root on thickness (Fig. 3).

(2) In both cases, for an infinitely thin sample thickness, the extrapolated wavelength corresponds to a photon energy of 2.52 ± 0.03 eV.

(3) The position of the maximum derivative around the transmission edge for the B5 sample investigated in Ref. 10 seems to match (visually) that of the 940 µm thick sample [Fig. 2(b)]. Assuming that the linear dependence also holds for this sample, a thickness of 940 ± 8 µm can then be extrapolated for the B5 sample investigated in Ref. 10 (see Fig. 3).

A possible explanation of the 500 nm edge shift resulting from the grinding of sample B5 could be the release of internal stresses with thinning, since a shift toward lower wavelengths with increasing annealing temperature (900 °C in ambient air for 18 h) has also been reported in Ref. 10. Conversely, the shift of this "blue edge" toward higher wavelengths with increasing fluence, i.e., due to defects induced by electron irradiation in MT-04 samples (Fig. 1), seems to substantiate such an explanation. Considering the bulk effect of such internal stresses, it sounds reasonable to expect an almost linear dependence of the edge shift on thickness.

Nonetheless, the spectra of B5 (Ref. 10) and new B5-940 samples exhibit slight differences despite their similar thickness. Indeed, an extra transmission edge seems to occur at around 900 nm for the former sample as opposed to the latter. This might be caused by their different microstructures, because both samples have been cut at different locations from the grown ZnO boule.

The transmission of one B5 sample has been measured in Prague within the wavelength range of 340– 850 nm and found to be very similar to that published in Ref. 10.

From the plot of the squared absorption coefficient α^2 versus photon energy E, it is possible to obtain the optical bandgap energy E_g^{opt}. This is based on the fact that in so-called direct bandgap semiconductors the joint density of states of electrons and holes gives the absorption coefficient α which is initially proportional to $(h\nu - E_g^{opt})^{1/2}$, as the conduction and valence bands are almost parabolic in the

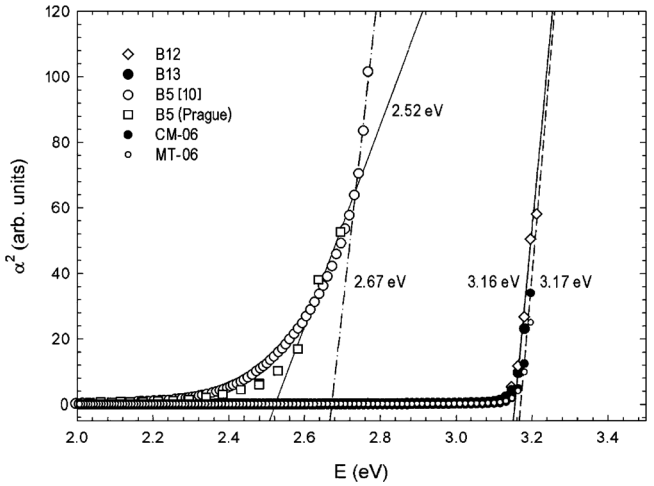

FIG. 4. Square of the absorption coefficient α plotted versus photon energy *E* of samples B12, B13, B5 (Ref. 10), B5 (squares: additional measurements performed in Prague), CM-06, and MT-06. Derived E_g^{opt} value is also given.

vicinity of the band edges,[30] *hv* being the photon energy. While this type of approach may be considered somewhat arbitrary, it has already been validated for GaAs (Ref. 31) and ZnO.[32–36] Its application to the transmission data from Fig. 1 taken in the broadest wavelength range available (200–2500 nm) gave the results shown in Fig. 4.

For sample B5 a value of $E_g^{opt} = (2.67 \pm 0.12)$ eV was derived. The large error bar accounts for the uncertainty in defining a common slope to B5 (Ref. 10) and B5 (Prague measurement). This numerical value is close to the energy extrapolated for the transmission for the B5 sample series (Fig. 3). Indeed, within the blue edge domain, the product of the absorption coefficient (α) by the thickness (*x*) (i.e., the exponent of the transmission exponential factor) should be dimensionless. Therefore we expect α and *x* to follow a reciprocal dependence on energy, and intrinsic optical properties to prevail when the thickness tends to zero. The various E_g^{opt} values derived from this approach are collected in Table III together with values estimated in Refs. 32–36.

The difference between the nominal bandgap $E_g = 3.37$ eV at 300 K known for ZnO (Refs. 1–3) and the E_g^{opt} values given in Table III indicates the presence of optically active defects in all samples. This means that the corresponding defects are characterized by this energetic amount from either the valence or conduction band within the bandgap.

In the case of the results presented in Ref. 32, the authors suggested formation of fluorine atoms substituting oxygen during growth, which results in fluorine atoms having the charge state {−1}. In Ref. 34, the authors concluded that oxygen vacancies (V_O) were present, because they found in their ZnO films that E_g^{opt} decreases with increasing oxygen pressure during deposition.

For sample B5, (E_g - E_g^{opt}) yields a relatively large value of 0.70 eV. Indeed, such a value (~0.7 eV) has already been reported[37] from previous PAS investigations in combination with optical absorption studies. The corresponding shift of the optical absorption bandedge and the reddish color were thereby induced by annealing of ZnO crystals either in Zn or Ti vapor and concluded to be due to the formation of

TABLE III. Estimated E_g^{opt} values for various ZnO samples from this work and the literature (Refs. 32–36).

Sample	Growth Method	Egopt/eV	Reference
B12	Bridgman Method	3.16 ± 0.02	This work (Fig. 4)
B13	Bridgman Method	3.16 ± 0.02	This work (Fig. 4)
B5	Bridgman Method	2.52 ± 0.03	This work (Fig. 3)
B5	Bridgman Method	2.67 ± 0.12	This work (Fig. 4)
CM-06	Pressurized Melt Growth	3.17 ± 0.03	This work (Fig. 4)
MT-06	Hydrothermal Growth	3.17 ± 0.03	This work (Fig. 4)
ZnO crystal	Bridgman Method	3.21	32
ZnO thin film	Sol-Gel Deposition	3.26	33
ZnO thin film	Molecular Beam Epitaxy	3.26	34
ZnO thin film	Magnetron Sputtering	3.26	35
ZnO thin film	Spray Pyrolysis	3.26	36

V_O. A shift of the optical edge by 0.7 eV was discussed earlier by Halliburton *et al.* in Ref. 38. However, Ref. 37 linked the shift to oxygen vacancies and excluded zinc interstitials whereas Halliburton *et al.* in Ref. 38 could not draw this distinction.

The orange coloration of ZnO was attributed to the presence of V_O in Refs. 37 and 39, it was concluded that zinc interstitials (Zn_i) were not the donors in as-grown ZnO - rather, that an H atom trapped in V_O, called the H_O defect, [40] forms multicenter bonds and thus acts as shallow donor.

Furthermore, it is appealing to consider the disposition of Zn_i which can be present at high concentration in ZnO grown in Zn-rich conditions. In Ref.41 it is assumed that these Zn_i defects form at octahedral lattice sites with a positive charge state {+2} and with a formation energy of $E_f = 0.87$ eV. Hence, it is reasonable to suppose that the light absorbers in sample B5 could also be finely dispersed Zn_i which then condensate either in the form of nanometer-sized (diameter ~3 nm) metallic precipitates[42] or by the generation of stacking faults (SF's) characterized by an additional (0002) plane.[43]

It is important to emphasize that the formation of a SF would require the precipitation of a double layer consisting of zinc and oxygen atoms. Thus, if only Zn_i occur in an excess concentration, oxygen atoms would have to diffuse from the surrounding lattice to form a complete (0002) double layer. As a consequence, a high concentration of V_O should be found in the vicinity of a SF. However, these defects might be 'invisible' to positrons because they form a H_O defect, the occurrence of which has been extensively discussed in the literature[13,40,44] and experimentally investigated (see for example, Refs. 15, 45 and 46 and references given therein). If the H atomic bond is strong enough so as not to be broken by energy transfer during NRA, its maximum concentration in the ZnO crystals can be estimated from the NRA results, which give the amount of H-b to be of the order 0.3 at.-% or even higher.[9]

The annealing of an optically transparent ZnO crystal grown by seeded chemical vapor transport in zinc vapor at 1100 °C for 30 min has been found to convert its color to deep red.[38] The optical absorption edge was observed to shift from ~400 nm to ~500 nm, corresponding to a shift of the optical edge by 0.7 eV. The observed increase in the number

of free carriers was proposed to be a result of either (1) the formation of Zn_i or (2) having the ground state of the neutral V_O near the conduction band. Interestingly, from this conclusion the coexistence of V_O and Zn_i after coloration is not excluded.

It was suggested in another recent work[47] that Zn_i and V_O can coexist. The authors have shown that the interactions between defects lead to a significant reduction in their formation energies, if the concentration of intrinsic defects becomes sufficiently high in O-deficient ZnO. Hence, the formation of both V_O and Zn_i becomes significantly enhanced by a strong attractive interaction between them, making these defects an important source of *n*-type conductivity in ZnO.

According to Ref. 37, Zn_i is not the cause of the coloration of ZnO but is most probably connected with the presence of V_O,[37–39] which however is 'invisible' to positrons. On the other hand, Zn_i are not expected to be stable at room temperature but highly mobile (see Ref. 48 and references therein). Its disposition in ZnO crystals remains to be determined and one can only consider which configurations might eventually explain the positron lifetime of 165-167 ps observed both in colorless MG ZnO crystals[9] and our brownish B5 sample. In our opinion, a possible complex formed between a Zn_i and a nitrogen atom replacing an oxygen atom in the crystal lattice (Zn_i - N_O) (Ref. 49) is not capable of trapping a positron.

In a very recent work,[46] H_O were again identified as the color-changing defects in ZnO and the presence of Zn_i and V_{Zn} was ruled out. This finding is not in contradiction to the supposed existence of SF's, which possibly might trap positrons and thus be able to explain the 165-167 ps positron lifetime. Hence, the SF's are anticipated to exist in a sufficiently large concentration in MG ZnO crystals independent of their coloration. The difference between colorless and brownish crystals would thus be caused just by the V_O or H_O defects located at the SF.

C. Microstructure analysis using XRD and TEM

The main goals of the microstructure analysis were (1) to verify the presence of stacking faults that are expected to be capable of explaining the positron lifetime of 165-167 ps observed in MG samples and (2) to identify the differences in the microstructure of the MG and HTG samples that could be responsible for the differences in the positron lifetime and in the optical bandgap energy.

XRD measurements performed on MG samples (B5 and B13) confirmed their single-crystalline nature. No traces of crystalline Zn were found that could be regarded as a constituent of the precipitates, which were recognized by optical absorption (see Sec. III B). The only indicator of the existence of precipitates (of unknown chemical composition) is the intense diffuse scattering in the overview XRD pattern (Fig. 5). However, the diffuse scattering arises generally on strain fields in crystal lattices.

The differences in the microstructures of MG samples were found to be rather small. The analyzed volume of sample B13 consisted of two mosaic blocks having the mutual

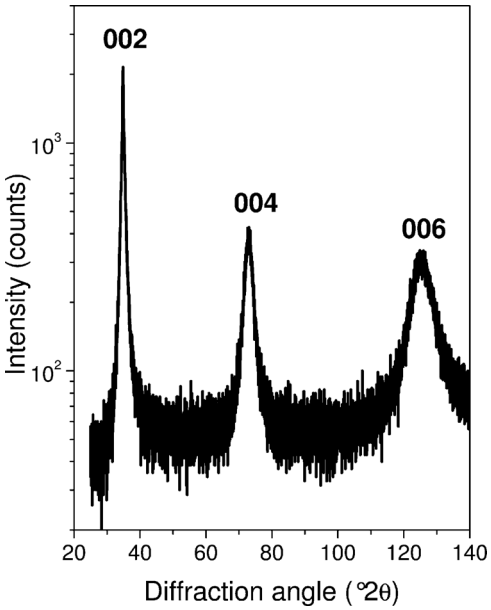

FIG. 5. Overview XRD pattern of sample B13 taken in symmetrical diffraction geometry on a Bragg-Brentano diffractometer.

disorientation of approximately 0.27°. This disorientation was calculated from the distance of two distinct diffraction maxima observed along q_x in the reciprocal space map of the diffraction line 002 (see Fig. 6). The angular scale was recalculated into the components of the reciprocal space vectors (q_x and q_z) according to:

$$\begin{aligned} q_x &= \tfrac{2\pi}{\lambda}[\cos(\Theta-\Omega)-\cos(\Theta+\Omega)] \\ q_x &= \tfrac{2\pi}{\lambda}[\sin(\Theta-\Omega)-\sin(\Theta+\Omega)] \end{aligned} \quad (1)$$

where Θ is the Bragg angle of the diffraction line under consideration and Ω the inclination of the sample from the symmetrical position. For a constant Θ and a small difference in Ω, it follows from Eq. (1) that the distances in the angular space and in the reciprocal space are directly proportional to each other:

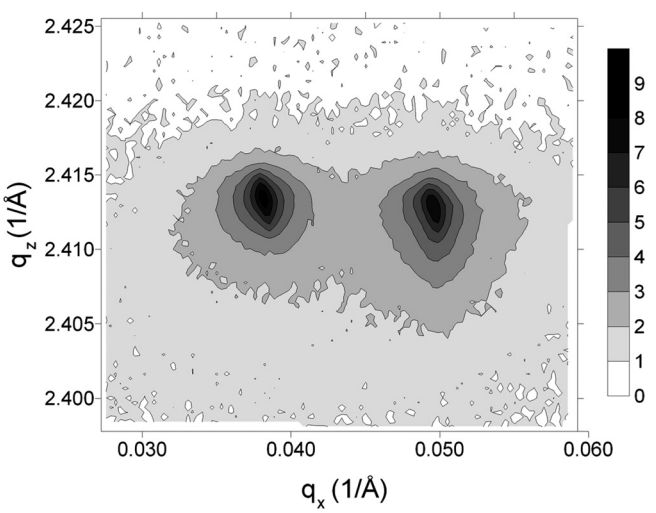

FIG. 6. Reciprocal space map measured for sample B13 in the vicinity of the reciprocal lattice point 002. The intensities are plotted in logarithmic scale.

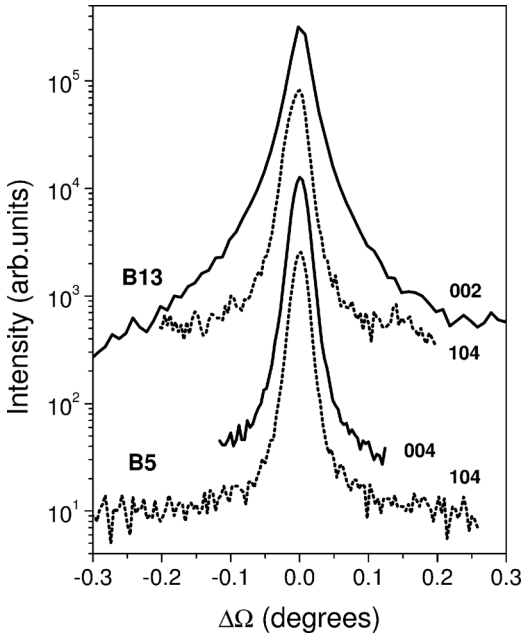

FIG. 7. Sample scans (Ω scans) taken on the diffraction lines 002, 004 (solid lines) and 104 (dotted lines) in MG samples B5 (lower curves) and B13 (upper curves).

$$\Delta q_x = \frac{2\pi}{\lambda}[\sin(\Theta - \Omega) + \sin(\Theta - \Omega)]\Delta\Omega \qquad (2)$$

According to Eq. (2), the above distance between the diffraction maxima ($\Delta\Omega = 0.27°$) corresponds to $\Delta q_x = 0.0113$ Å^{-1} (cf. Fig. 6). In sample B5, no such disorientation was observed within the analyzed volume. The mean disorientation of lattice planes within individual mosaic blocs was below 60 arcsec in both MG samples as concluded from the full-widths at the half maximum (FWHM) of the reflections 002, 004 and 104, which were measured as Ω scans (Fig. 7). However, as the FWHM recalculated into q_x do not change significantly with the length of the diffraction vector, the instrumental line broadening and natural width of the Darwin curve can be regarded as more probable reasons for the observed line broadening in the q_x direction than the microstructure defects.

On the contrary, the XRD line broadening measured in the MG samples along q_z increases with the size of the diffraction vector that indicates inhomogeneous changes of the interplanar spacing and consequently the presence of local lattice strains. Moreover, diffraction lines are strongly asymmetric in the q_z direction, which suggests that the sources of the inhomogeneous changes of the interplanar spacing are stacking faults.[50]

Another indicator of the presence of stacking faults, and their different density in the MG samples, is a slight difference in the lattice parameters determined for samples B5 and B13: $a(B5) = 0.32530(2)$ nm, $c(B5) = 0.52069(2)$ nm, $a(B13) = 0.32571(2)$ nm and $c(B13) = 0.52057(2)$ nm. The elementary cell volumes determined from these lattice parameters also differ; the elementary cell of sample B5 (47.72×10^{-3} nm^3) is smaller than that of sample B13 (47.83×10^{-3} nm^3).

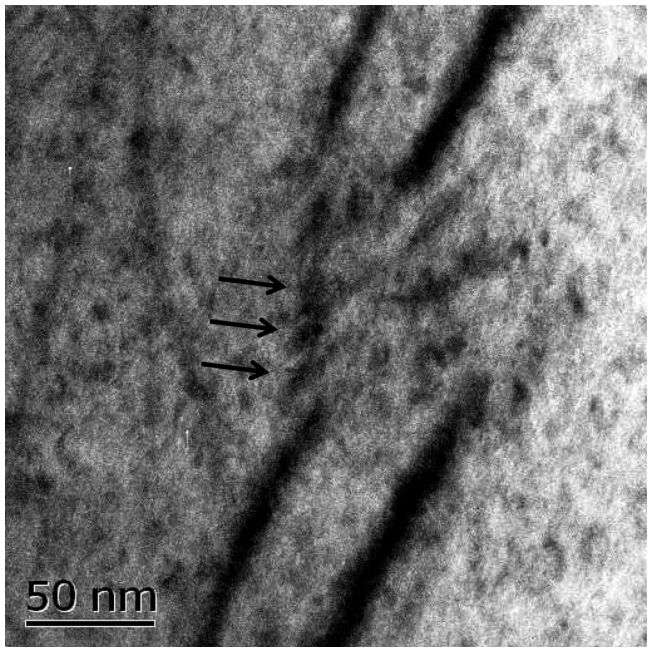

FIG. 8. TEM micrograph of sample B5 taken in diffraction contrast. The arrows indicate some examples of the diffraction contrast from the strain fields induced by stacking faults.

The extrapolation of the XRD line broadening to $q_z = 0$ yielded FWHM ≈ 36 arcsec, which excludes any line broadening due to the size of the mosaic blocks. Local lattice strains that are related to the inhomogeneous changes of the interplanar spacing and that are anticipated to stem from the stacking faults are illustrated in the TEM micrograph given in Fig. 8. Moreover, Fig. 8 reveals a rough estimation of the density of these microstructure defects. However, one has to keep in mind that only microstructure defects with a certain orientation to the diffraction vector are visible for TEM

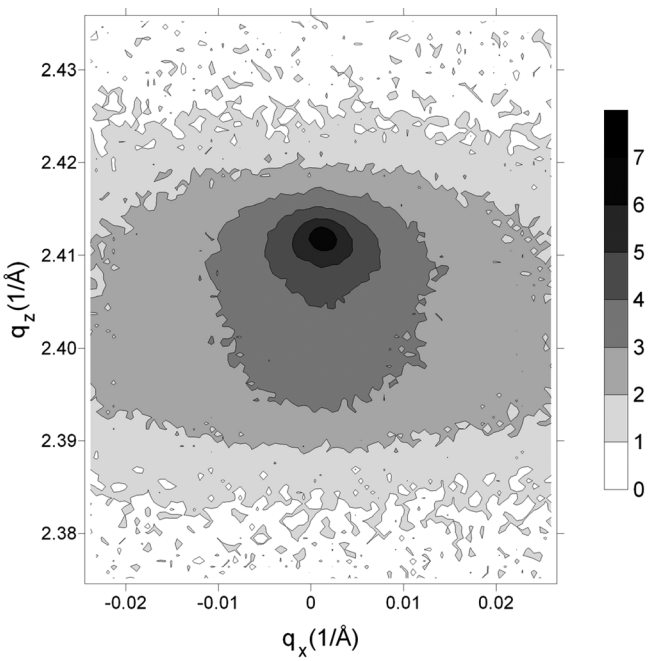

FIG. 9. Overview XRD pattern of sample MT-08 measured in symmetrical diffraction geometry on a Bragg-Brentano diffractometer.

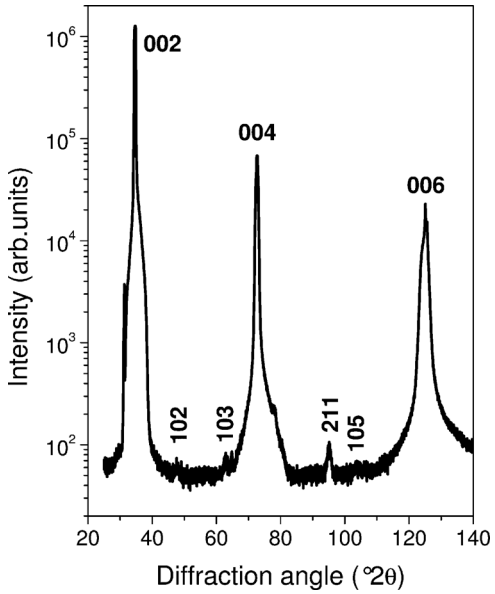

FIG. 10. Reciprocal space map taken for sample MT08 in the vicinity of the reciprocal lattice point 002. The intensities are plotted in logarithmic scale.

performed in diffraction contrast. Thus, the real density of the microstructure defects is assumed to be higher than the defect density depicted in Fig. 8.

In the HTG sample (MT-08), a minor fraction of crystalline domains of ZnO with other orientations was found (Fig. 9). These small and almost randomly oriented crystallites fragmented the ZnO domains with the dominant crystallographic orientation. Thus, the effect of the crystallite size on the line broadening along q_z could be seen in this particular sample. The estimated size of the domains with the dominant orientation was between 200 and 260 nm. Furthermore, the presence of differently oriented domains and the fragmentation of the crystal caused the highest diffuse scattering among the samples under study (Fig. 10). Sample MT-08 possesses the lattice parameter within the basal plane $a = 0.32552(2)$ nm and the highest lattice parameter c among the samples under study, $c = 0.52074(2)$ nm. The corresponding volume of the elementary cell is 47.79×10^{-3} nm^3.

VI. CONCLUSIONS

Measurements of conventional positron lifetime and optical transmission of various nominally undoped, hydrothermally (HTG) or melt grown (MG) ZnO single crystals have been presented together with their structural characterizations by X-ray diffraction and transmission electron microscopy. In addition, the content of bound hydrogen (H-b) of a brownish MG ZnO single crystal (sample B5) has been estimated to H-b $= (0.30 \pm 0.03)$ at.-%.

The positron lifetime of the sample B5 was found to match perfectly the 165-167 ps positron lifetime of colorless MG ZnO crystals. Its optical absorption edge shift was estimated to be 0.70 eV, which is comparable with values reported previously in literature.[37,38]

The disposition of excess Zn_i, which can be present at high concentration in ZnO grown in Zn-rich conditions as discussed in the literature, has been summarized. As a result, it was proposed to investigate if SF's generally exist in a sufficiently large concentration in MG ZnO crystals to explain the 165-167 ps positron lifetime range observed.[9]

From careful, comparative XRD investigations it has been concluded that the presumed presence of Zn_i in the form of nanometer-sized (diameter ~3 nm) metallic precipitates[10] in the new brownish sample B5 is very unlikely, in contrast to another brownish sample from the same grown boule (B5).[42] The only indicator of the existence of precipitates observed here was the intense diffuse scattering in the overview XRD pattern, which however could originate from the lattice strain fields in the vicinity of the anticipated SF's.

The combined discussion of XRD and TEM analyses led to the conclusion that SF's are present in MG crystals in high concentrations, which suggests that this defect to be responsible for the observed positron lifetime of 165-167 ps. The difference from the positron lifetime observed in HTG ZnO crystals [180-182 ps (Ref. 9)] is understandable because SF's represent two-dimensional positron traps which usually exhibit shorter positron lifetimes than real open volume defects including $V_{Zn} + 1H$ complexes. Positrons are attracted to SF's due to their lowered atomic density compared to the bulk material.

ACKNOWLEDGMENTS

Financial support from the Research Grant Council of Hong Kong (HKU7031/08P and G_HK026/07) and German Academic Exchange Service (DAAD: D/08/01769) for cooperation visits between University of Hong Kong and Forschungszentrum Dresden-Rossendorf in 2008/2009 is gratefully acknowledged. A part of the work was performed within the Cluster of Excellence "Structure Design of Novel High Performance Materials via Atomic Design and Defect Engineering (ADDE)" that is financially supported by the European Union and by the Ministry of Science and Art of Saxony (SMWK). The support provided by the Ministry of Schools, Youths and Sports of the Czech Republic through the research plan MSM 0021620834 is also appreciated.

[1]D. C. Look, J. Mater. Sci. Eng. **80**, 383 (2001).
[2]Ü. Özgür, Y. I. Alivov, C. Lin, A. Teke, M. A. Reshchikov, S. Doğgan, V. Avrutin, S. - J. Cho and H. Morkoç, J. Appl. Phys. **98**, 041301 (2005).
[3]S. J. Pearton, D. P. Norton, K. Ip, Y. W. Heo, and T. Steiner, Prog. Mater. Sci. **50**, 293 (2005).
[4]S. Dutta, S. Chattopadhyay, A. Sarkar, M. Chakrabarti, D. Sanyal, and D. Jana, Prog. Mater. Sci. **54**, 89 (2009).
[5]Positron Spectroscopy of Solids, edited by A. Dupasquier and A. P. Mills, Jr (IOS, Amsterdam, 1995).
[6]R. Krause-Rehberg and H. S. Leipner, *Positron Annihilation in Semiconductors - Defect Studies*, (Springer, Berlin, 1999).
[7]Slow Positron Beam Techniques for Solids and Surfaces, edited by G. Brauer and W. Anwand, (ELSEVIER, Amsterdam, 2002).
[8]R. I. Grynszpan, W. Anwand, G. Brauer, and P. G. Coleman, Ann. Chim. (Paris) **32**, 365 (2007).
[9]G. Brauer, W. Anwand, D. Grambole, J. Grenzer, W. Skorupa, J. Čížek, J. Kuriplach, I. Procházka, C. C. Ling, C. K. So, D. Schulz, and D. Klimm, Phys. Rev. B **79**, 115212 (2009).
[10]D. Schulz, S. Ganschow, D. Klimm, M. Neubert, M. Roβberg, M. Schmidbauer, and R. Fornani, J. Cryst. Growth **296**, 27 (2006).
[11]M. G. Wardle, J. P. Goss, and P. R. Briddon, Phys. Rev. Lett. **96**, 205504 (2006).
[12]N. H. Nickel, Phys. Rev. B **73**, 195204 (2006).
[13]H. Takenaka and D. J. Singh, Phys. Rev. B **75**, 241102(R) (2007).

[14]J. Cizek, N. Zaludova, M. Vlach, S. Danis, J. Kuriplach, I. Prochazka, G. Brauer, W. Anwand, D. Grambole, W. Skorupa, R. Gemma, R. Kirchheim, and A. Pundt, J. Appl. Phys. **103**, 053508 (2008).
[15]E. A. Lavrov, Physica B **404**, 5075 (2009).
[16]E. V. Monakhov, A. Yu. Kuznetsov, and B. G. Svensson, J. Phys. D: Appl. Phys. **42**, 153001 (2009).
[17]W. Anwand, G. Brauer, T. E. Cowan, D. Grambole, H. Schmidt, W. Skorupa, J. Cizek, J. Kuriplach, I. Prochazka, W. Egger, and P. Sperr, Phys. Status Solidi. A **207**, 2415 (2010).
[18]D. C. Reynolds, C. W. Litton, D. C. Look, J. E. Hoelscher, B. Claflin, T. C. Collins, J. Nause, and B. Nemeth, J. Appl. Phys. **95**, 4802 (2004).
[19]J. Nause and B. Nemeth, Semicond. Sci. Technol. S **45** (2005).
[20]W. A. Lanford, "Nuclear Reactions for Hydrogen Analysis," in Handbook of Modern Ion Beam Materials Analysis, edited by R. Tesmer and M. Nastasi, (Materials Research Society, Pittsburgh, 1995) p. 193.
[21]G. Brauer, W. Anwand, D. Grambole, W. Skorupa, Y. Hou, A. Andreev, C. Teichert, K. H. Tam, and A. B. Djurišić, Nanotechnology **18**, 195301 (2007).
[22]J. F. Ziegler, J. P. Biersack, and U. Littmark, *The Stopping and Range of Ions in Solids* (Pergamon, New York, 1985).
[23]F. Bečvář, J. Čižek, L. Lestak, I. Novotny, I. Procházka, and F. Sebesta, Nucl. Instrum. Methods Phys. Res. A **443**, 557 (2000).
[24]I. Procházka, I. Novotny, and F. Bečvář, Mater. Sci. Forum 255–257, **772** (1997).
[25]G. Brauer, W. Anwand, W. Skorupa, J. Kuriplach, O. Melikhova, J. Čižek, I. Procházka, C. Moisson, H. von Wenckstern, H. Schmidt, M. Lorenz, and M. Grundmann, Superlattices Microstruct. **42**, 259 (2007).
[26]E. H. Kisi and M. M. Elcombe, Acta Crystallogr. **45**, 1867 (1989).
[27]G. Brauer, W. Anwand, W. Skorupa, J. Kuriplach, O. Melikhova, C. Moisson, H. von Wenckstern, H. Schmidt, M. Lorenz, and M. Grundmann, Phys. Rev. B **74**, 045208 (2006).
[28]G. Mie, Ann. Phys. **25**, 377 (1908).
[29]P. W. Barber and S. S. Hill, *Light Scattering by Particles: Computational Methods* (World Scientific, Singapore, 1990).
[30]J. Singleton, "Band Theory and Electronic Properties of Solids," in *Oxford Master Series in Condensed Matter Physics* (Oxford University Press, Oxford, 2001).
[31]M. D. Sturge, Phys. Rev. **127**, 768 (1962); **127**, 768 (1962).
[32]X.-H. Li, J.-Y. Xu, M. Jin, H. Shen, and X.-M. Li, Chin. Phys. Lett. **23**, 3356 (2006).
[33]A. Jain, P. Sagar, and R. M. Mehra, Solid-State Electron. **50**, 1420 (2006).
[34]C. Wang, Z. Chen, H. Hu, and D. Zhang, Physica B **404**, 4075 (2009).
[35]Y. Chen, X. L. Xu, G. H. Zhang, H. Xue, and S. Y. Ma, Physica E **42**, 1713 (2010).
[36]F. Yakuphanoglu, Y. Caglar, S. Ilican, and M. Caglar, Physica B **394**, 86 (2007).
[37]F. A. Selim, M. H. Weber, D. Solodovnikov, and K. G. Lynn, Phys. Rev. Lett. **99**, 085502 (2007).
[38]L. E. Halliburton, N. C. Giles, N. Y. Garces, M. Luo, C. Xu, L. Bai, and L. A. Boatner, Appl. Phys. Lett. **87**, 172108 (2005).
[39]S. Lany and A. Zunger, Phys. Rev. B **78**, 235104 (2008).
[40]A. Janotti and C. G. Van de Walle, Nature Mater. **6**, 44 (2007).
[41]A. F. Kohan, G. Ceder, D. Morgan, and C. G. Van de Walle, Phys. Rev. B **61**, 15019 (2000).
[42]K. Irmscher, M. Albrecht, B. Heimbrodt, M. Naumann, T. Remmele, D. Schulz, T. Schulz, and R. Fornari, Phys. Status Solidi C **6**, 2658 (2009).
[43]D. Gerthsen, D. Litvinov, Th. Gruber, C. Kirchner, and A. Waag, Appl. Phys. Lett. **81**, 3972 (2002).
[44]A. Janotti and C. G. Van de Walle, Rep. Prog. Phys. **72**, 126501 (2009).
[45]E. V. Lavrov, F. Herklotz, and J. Weber, Phys. Rev. B **79**, 165210 (2009).
[46]M. H. Weber, N. S. Parmar, K. A. Jones, and K. G. Lynn, J. Electro. Mater. **39**, 573 (2010).
[47]Y. - S. Kim and C. H. Park, Phys. Rev. Lett. **102**, 086403 (2009).
[48]M. D. McCluskey and S. J. Jokela, J. Appl. Phys. **106**, 071101 (2009).
[49]D. C. Look, G. C. Farlow, P. Reunchan, S. Limpijumnong, S. B. Zhang, and K. Nordlund, Phys. Rev. Lett. **95**, 225502 (2005).
[50]B. E. Warren, *X-ray Diffraction*, (Dover Publishers, New York, 1990).